Edwards-Wilkinson depinning transition in random Coulomb potential background

N. Valizadeh,[1] M. Samadpour,[1] H. Hamzehpour ⊙,[1] and M. N. Najafi[2,*]

[1]*Department of Physics, K.N. Toosi University of Technology, Tehran 15875-4416, Iran*
[2]*Department of Physics, University of Mohaghegh Ardabili, P.O. Box 179, Ardabil, Iran*

The quenched Edwards-Wilkinson growth of the $1+1$ interface is considered in the background of the correlated random noise. We use random Coulomb potential as the background long-range correlated noise. A depinning transition is observed in a critical driving force $\tilde{F}_c \approx 0.037$ (in terms of disorder strength unit) in the vicinity of which the final velocity of the interface varies linearly with time. Our data collapse analysis for the velocity shows a crossover time t^* at which the velocity is size independent. Based on a two-variable scaling analysis, we extract the exponents, which are different from all universality classes we are aware of. Especially noting that the dynamic and roughness exponents are $z_w = 1.55 \pm 0.05$, and $\alpha_w = 1.05 \pm 0.05$ at the criticality, we conclude that the system is different from both Edwards-Wilkinson (EW) and Kardar-Parisi-Zhang (KPZ) universality classes. Our analysis shows therefore that making the noise long-range correlated, drives the system out of the EW universality class. The simulations on the tilted lattice show that the nonlinearity term (λ term in the KPZ equations) goes to zero in the thermodynamic limit.

I. INTRODUCTION

The growth of rough interfaces in random media has absorbed much attention due to its vast application in the fluid dynamics in porous media [1–3]. The wettability and the disorder are two factors which along with the driving force give the dynamics of the interfaces [4–6]. Several authors in the past have focused on multiphase flow in mixed wet porous media, and discovered clear discrepancies in the fluid behavior in uniform wet systems and in mixed wet systems [7–11]. Also, much attention was paid to the dynamics associated with a Haines jump [12], the interface of fluid and porous structures using the smoothed particle hydrodynamics model [13], the propagation of a reaction front inside a porous medium [14], depinning and dynamics of imbibition fronts in the paper under increasing ambient humidity [15], lattice models for flow in porous media [16], fluid-fluid displacement [9,10,12,17–19], fire front motion [20], and motion of flux lines in superconductors [21]. Magnetic domains [22] and evolution of cell colony fronts [23] are other examples of the growth of rough interfaces in random media. An important large class of interface dynamics is the ones that are pushed, and at the same time get pinned at random obstacles already present in the host media. The stochasticity of the dynamics of these interfaces is due to the latter, which originates from the stochasticity of the obstacles, i.e., their size, permeability, etc. Generally, the properties of the interfaces depend on two ingredients [24]: the dynamical laws governing the interfaces and the pattern of the quenched disorder present in the host media. The effect of the governing laws has been vastly studied in the literature [25]. The depinning transition phenomenon is one

of the important observations in this field, which is defined as a point that the system changes behavior from being pinned to obstacles (which is identified by a zero interface velocity at long times), to a moving phase (nonzero interface velocity at long times). This second-order transition, for which there is much experimental and theoretical evidence, is due to the nonlinearity of these systems, and the competition between the driving force and the resistance force due to the obstacles [6]. On the theoretical side, there are two general approaches for modeling these systems: continuous and discrete models which are classified based on the critical exponents in the vicinity of the transition. Quenched Edwards-Wilkinson (QEW) and Kardar-Parizi-Zhang (KPZ) classes are the most famous continuous models, and the directed percolation depinning class is one of the most important discrete models. For a good classification of the models, see [6,25]. Many aspects and applications of these models were studied in the literature [14,25–32]. Despite this huge literature, little work has been done on the effect of the type of the quenched noise (mainly correlated vs uncorrelated) in the host media. In most applications, the authors concentrated on the quenched disorders which are realized by the uncorrelated noises in a given range. Nature may behave in a more complicated way, i.e., the disorder can be correlated in various ways which should be realized by the models which contain the key parameters as in the original system.

Correlated noises and also long-range correlations are ubiquitous in nature. Examples include the correlations that exist in the porosity [32–34], diffusion [35], and permeability [33,34,36,37] in porous media. Also many random systems are described in terms of or mapped to the random Coulomb potential (RCP), ranging from the free Bosonic system to the Edwards-Wilkinson (EW) model of surface growth process [38], inverse turbulence cascades [39], and the electric field

─────────
*morteza.nattagh@gmail.com

of randomly charged noise [40,41]. Here we focus on the opposite limit of uncorrelated noises, which is two-dimensional long-range correlated disordered systems. We use the RCP to model the quenched noise, which is a well-known model in statistical mechanics. Many properties of this model are known; for example, it is quite similar to the Edwards-Wilkinson model in the stationary phase [40,41], which itself is $c = 1$ conformal field theory [42] in two dimensions, and Coulomb gas [43]. From the global point of view, the interfaces of this model are described by Schramm-Lowener evolution with the diffusivity parameter $\kappa = 4$ [43]. The host media which is governed by RCP is long range since the correlation of fields is logarithmic (equivalent to the zero roughness exponent in the EW model) and therefore the corresponding noise is quite long range [44,45]. Previously some dynamical models combined with a random Coulomb potential model, like the percolation [41] and the Ising [40].

In this paper we consider the depinning transition governed by the QEW model on top of a media for which the correlation of the noise is controlled by RCP. We find that the properties of the depinning transition change significantly by introducing the RCP correlations. In particular, we see a new type of two-parameter scaling relation around the critical driving force $F = F_c$.

The paper is organized as follows: In the next section, we explore the main properties of the depinning transitions. The general setup of the RCP noise in our paper is presented in Sec. III. Section IV is devoted to the presentation of our results. We close the paper with a conclusion.

II. GENERAL PROPERTIES OF DRIVEN INTERFACES

We study the driven interface dynamics in two-dimensional random media as its background, represented by stochastic obstacles, whose positions and strengths are correlated. The problem is $2 + 1$ dimensional, where two spatial components are (x, y), and 1 stands for the time t. We especially concentrate on the motion pattern of one-dimensional interface $y = h(x, t)$, the border between "dry" and "wet" phases, in the presence of "quenched noise" $\eta(x, y)$ distributed over the space, and also driving force (here represented by F). For small enough driving forces the interface is shown to be in the "pinned" phase in which the interface stops, more precisely $\bar{h}(t) \equiv \sum_{x=1}^{L} h(x, t)$ (where L is system size) vanishes at large enough time due to the obstacles, meaning that the disordered resistance force is statistically more effective than the driving force. For large enough F's the interfaces are in the "moving" phase. There is a critical value of F, represented by F_c where the interface undergoes a transition from the pinned phase to the moving phase, named the depinning transition. Let us define the average velocity of the interface by

$$\bar{v}_F(t, L) = \frac{\partial \langle \bar{h} \rangle}{\partial t}, \tag{1}$$

where the $\langle \cdots \rangle$ is the ensemble average. The order parameter of the depinning transition is then defined by $\bar{v}_\infty \equiv \lim_{t \to \infty} \frac{d}{dt} \bar{h}$, i.e., $\bar{v}_\infty = 0$ for the pinned phase, and $\bar{v}_\infty > 0$ for the moving phase. When $\eta(x, h(x, t))$ is an uncorrelated quenched random noise, and the governing equation is the EW, not surprisingly the underlying interface at F_c becomes a

self-similar (more precisely self-affine) extended object with critical properties similar to the one-dimensional EW universality class. In this case, many statistical observables display scaling behaviors. An example is the interface width, which has become a standard tool in the study of growing surfaces for various theoretical and experimental models of growing interface. It characterizes the roughness of the interface, and is defined by the fluctuations of the height field. It is defined by

$$w^2 = \overline{\langle (h(\mathbf{r}) - \bar{h})^2 \rangle}, \tag{2}$$

where the overbar represents the spatial average $\overline{O} \equiv \frac{1}{L} \sum_i O(x = i)$. For the EW model it is well known that there is a crossover timescale t_X. For $t \leqslant t_X$ the width increases as a power of time $w(L, t) \sim t^{\beta_w}$, where the exponent β_w is called the growth exponent and characterizes the time-dependent dynamics of the roughening process. The power-law increase of width does not continue indefinitely, but is followed by a saturation regime (for $t \geqslant t_X$) during which the width reaches a saturation value, w_{sat}. Indeed w_{sat} itself scales with L^{α_w}; the exponent α_w being called the roughness exponent, is a second critical exponent that characterizes the model. The timescale t_X depends on L in a power-law fashion $\sim L^{z_w}$, where the dynamic exponent z_w is equal to $\frac{\beta_w}{\alpha_w}$. These relations are summarized in a famous scaling relation for the interface width, w, as well as some other statistical quantities [25,46–55]

$$w(L, t) = L^{\alpha_w} F_w\left(\frac{t}{L^{z_w}}\right) = t^{\alpha_w/z_w} G_w\left(\frac{t}{L^{z_w}}\right) \tag{3}$$

from which the exponents can be extracted. The functions $F_w(x)$ and $G_w(x) = x^{-\alpha_w/z_w} F(x)$ (showing that $z_w = \frac{\alpha_w}{\beta_w}$) are some universal functions with the asymptotic behavior $F_w(x) = \begin{cases} x^{\beta_w} & x \ll 1 \\ \text{const.} & x \gg 1 \end{cases}$.

For $1 + 1$ EW the exponents are $\alpha_w = 0.5$, $\beta_w = 0.25$, and $z_w = 2$, whereas for QEW we have $\alpha_w = 0.92(4)$, $\beta_w = 0.85(3)$, and $z_w = 1.08(1)$.

For the QEW class at $F = F_c$ the average velocity $\bar{v}_F(t)$ decreases with time in a power-law fashion [23]

$$\bar{v}_F(t) \sim t^{-q}, \tag{4}$$

whereas $\bar{v}_F(t) \sim e^{-t/\xi_F}$ for $F < F_c$, where $\xi_F \sim |F - F_c|^{-\nu}$ and ν is called the correlation length exponent. In the vicinity of F_c, we have also

$$\bar{v}_\infty \sim f^\theta, \quad f \equiv \frac{F - F_c}{F_c}, \tag{5}$$

where $\theta > 0$ is the velocity exponent. Close to this transition, some parts of the interface are growing, and some parts are *pinned*, forming pinning paths, and the growth occurs by the propagation of these growing regions. Taking into account that the characteristic time required for this propagation is t_X (since it is the time required for correlations to propagate across the system), and the typical advance for each movement (from one blocking the path to the other) is w_{sat}, one obtains [6]

$$\bar{v}_\infty \propto \frac{w_{\text{sat}}}{t_X} \propto \zeta^\alpha / \zeta^z \propto f^{\nu(z-\alpha)} \tag{6}$$

giving us the hyperscaling relation $\theta = \nu(z - \alpha)$.

There are many experiments to realize the driven interfaces, like fluid-fluid displacement [17,56,57], imbibition of

coffee in paper towels [58–60], which reported scattered exponents for the critical driven interfaces [6]. Also, many effects in this field have been studied, such as $1/f$ noise in driven interfaces [61] and anomalous noise in driven interfaces [18]. Recently it was conjectured by Grassberger that critically pinned interfaces in two-dimensional isotropic random media with short-range correlations are always in the universality class of ordinary percolation [62]. There is a clever method to distinguish the universality classes of the driven interfaces, especially the KPZ universality class. If we start from a tilted initial configuration, i.e., $h_0 = mx$, then the final velocity behaves like

$$\bar{v}_\infty(m) = \bar{v}_\infty(m = 0) + \lambda m^2, \tag{7}$$

where $\bar{v}_\infty(m = 0) = \bar{v}_\infty \propto f^\theta$ scales with f as before, and $\lambda \sim f^\phi$, where $\phi < 0$ for the KPZ universality class, and $\phi > 0$ for the EW universality class. We see that

$$\bar{v}_\infty(m) \propto f^\theta + af^\phi m^2, \tag{8}$$

where a is an unimportant constant. It is worthy to note that these predictions are limited to the QEW and KPZ universality classes that are actually reductions of more sophisticated, more realistic models like the Darcy's model, which may show more complex behaviors. Given that λ is proportional to the nonlinearity coefficient in the KPZ model, one can see that the former is equivalent to a large nonlinearity term in the transition point governed by the KPZ class [46,63,64].

III. TWO-DIMENSIONAL RANDOM COULOMB POTENTIAL NOISE; OUR MODEL

In this section, we consider a two-dimensional host system with the correlated scale-invariant disorder. Correlated noises and also long-range correlations are ubiquitous in nature. Examples include the correlations that exist in the porosity [32–34], diffusion [35], permeability [33,34,36,37], and elastic constant, and wave speed [65] in porous media. RCPs are an important type of correlated disorder since many systems are mapped to them, such as free bosons and the EW model [38], inverse turbulence cascades [39], and the electric field of random charged noise [40,41]. Here we consider a different realization of RCP is the Poisson equation in the background of white-noise charge disorders, which itself is mapped to the EW model in the stationary state. We construct a correlated random (quenched) noise system, through which the driven interface moves. The governing equations of the interface dynamics are considered to be the ones for QEW equations. We can imagine this problem as the coupling of the driven interface problem with the random Coulomb potential model, or the critical phenomena on the fractal systems [66]. This concept can be extended to dilute systems that are fractal in some limits [67–71].

Before describing the problem in this type of media, let us first briefly introduce our method of generating RCPs shown by the field $\eta(\mathbf{r})$ to be used as a quenched noise in the dynamics of the driven interface. We consider a two-dimensional Poisson equation governing the $\eta(\mathbf{r})$

$$\nabla^2 \eta(\mathbf{r}) = -\rho(\mathbf{r}). \tag{9}$$

$\eta(\mathbf{r})$ is indeed a quenched spatial noise through which the interface moves. In this equation $\rho(\mathbf{r})$ is the spatial white noise with the normal distribution and the properties $\langle \rho(\mathbf{r}) \rangle = 0$ and $\langle \rho(\mathbf{r}) \rho(\mathbf{r}') \rangle = (n_i a)^2 \delta^3(\mathbf{r} - \mathbf{r}')$, n_i is the total density of Coulomb disorder and a is the lattice constant. This connection can be confirmed from both numerical and analytical levels. In the theoretical level, if one takes a look at the probability measure of Eq. (9), one finds that it is exactly the same as the probability measure of the EW in the stationary state (see Ref. [25]). On the numerical level also, we have seen that all of the statistical observables are the same. For example, the two-point correlations are logarithmic, the fractal dimension of isoheight contours is 1.5, the critical exponent of the gyration radius is 3.0, and the critical exponent of the loop lengths is 7/3 in accordance with the RCP [72]. It is well known that this model in the scaling limit is described by Gaussian distribution function [73]. It is also known that the contour lines of this model are described by the Schramm-Loewner evolution (SLE) theory with the diffusivity parameter $\kappa = 4$ [43], which is understood in terms of the conformal field theory (CFT)/SLE correspondence with the relation $c = (6 - \kappa)(3\kappa - 8)/(2\kappa)$. The fractal dimension of the contour loops $D_f^{\text{RCP}} = \frac{3}{2}$ which is also compatible with the relation $D_f = 1 + \frac{\kappa}{8}$. Before we proceed, it seems necessary to review some points: Actually the Poisson equation (9) with random uncorrelated noise is mapped onto the stationary state of the EW equation as explored in the literature. In this paper, we aimed to consider correlated quenched noises, which are described by self-similarity parameter α, quantifying the range of correlations. For this purpose, we found the EW model more appropriate than others, since for this case the correlations are logarithmic, i.e., $\langle \eta(\mathbf{r} + d)\eta(\mathbf{r}) \rangle \approx \log d$, which is more long range than other models in our list for which $\langle \eta(\mathbf{r} + d)\eta(\mathbf{r}) \rangle \approx d^\alpha$ with $\alpha > 0$. Therefore, the EW model fits our purpose (having long-range correlations) better than other models. All in all, we chose a two-dimensional Poisson equation with random uncorrelated charges as a representative of a stationary state of the EW model in two dimensions, employed to model the long-range-correlated quenched noise in our system. Please note that it should not be confused with the QEW model which was used to model the dynamics of the interface.

The probability distribution function of these fields transforms under $\mathbf{r} \to b\mathbf{r}$ as follows: scaling law

$$\eta(b\mathbf{r}) \stackrel{d}{=} b^{\alpha_{\text{RCP}}} \eta(\mathbf{r}), \tag{10}$$

where the parameter α_{RCP} is the *roughness* exponent or the *Hurst* exponent of the RCP and b is a scaling factor and the symbol $\stackrel{d}{=}$ means the equality of the distributions. The distribution of this system, like a wide variety of random fields, is Gaussian [72]. Various correlation functions [e.g., $C(r) \equiv \langle [\eta(\mathbf{r} + \mathbf{r_0}) - \eta(\mathbf{r_0})]^2 \rangle$], and the height total variance show power-law behavior [25], defining the roughness exponents of which are $\alpha = 0$. It is shown that [74] the probability distribution functions of this RCP noise are Gaussian:

$$P(V) \equiv \frac{1}{\sigma\sqrt{2\pi}} e^{-V^2/2\sigma^2}, \tag{11}$$

where σ is the standard deviation. In addition the contour loop ensemble can be characterized through the loop correlation function $G(\mathbf{r}) = G(r)$ ($r \equiv |\mathbf{r}|$) which is the probability measure of how likely the two points separated by the distance r lie on the same contour. For large distances this function scales with r as [72]

$$G(r) \sim \frac{1}{r^{2x_l}}, \tag{12}$$

where x_l is the loop correlation exponent. It is believed that the exponent x_l is superuniversal, i.e., for all the known monofractal Gaussian random fields in two dimensions, this exponent is equal to $\frac{1}{2}$ [72]. This model belongs to $c = 1$ CFT and also SLE$_4$.

We study the flow of a fluid in a two-dimensional random media as its background, represented by stochastic obstacles, whose positions and strengths are correlated as explained above [$\eta(\mathbf{r})$ in Eq. (9)]. The dynamics are governed by the QEW continuous growth equation. The system is $2 + 1$ dimensional, where two spatial components are $\mathbf{r} \equiv (x, y)$, and 1 stands for the time t. We especially concentrate on the motion pattern of one-dimensional interface $y = h(x, t)$, the border between "dry" and "wet" phases. The motion of $h(x, t)$ is governed by the QEW equation

$$\frac{\partial h(x, t)}{\partial t} = \upsilon \nabla^2 h(x, t) + F + \eta(x, h(x, t)). \tag{13}$$

where υ is the surface tension that is considered to be $\upsilon = 1$, and F is the driving force. It is worthy to note that a more complete description of fluid flow in porous media needs models like the Darcy model [70,75]. It is not simple to relate Darcy's nonlinear model to linear equation (13). One, however, can find such a mapping by considering Darcy's model for the frontier of the growing cluster where this frontier proceeds in the direction with the lowest pressure and considering a linear relationship between the rate of growth and the local gradient of pressure (see Darcy's law of velocity [70]).

In our simulations $\eta(\mathbf{r})$ belongs to $[-\eta_{\max}, \eta_{\max}]$ ($\eta_{\max} = 10$). One can normalize the equation so that the quantities are compared with unity using $\tilde{h}(\mathbf{r}) = \eta_{\max}^{-1} h(\mathbf{r})$, $\tilde{F} = \eta_{\max}^{-1} F$, and $\tilde{\eta}(\mathbf{r}) = \eta_{\max}^{-1} \eta(\mathbf{r})$, where $\eta_{\max}$ is the maximum η in the simulations, which gives

$$\frac{\partial \tilde{h}(x, t)}{\partial t} = \nabla^2 \tilde{h}(x, t) + \tilde{F} + \tilde{\eta}(x, y). \tag{14}$$

IV. RESULTS

We consider the time evolution of a rough $(1 + 1)$-dimensional interface described by the vertical coordinate $y = \tilde{h}(x, t)$ (the height of the interface at the horizontal position x and the time t). We start the simulation from $\tilde{h}(x, t) = 0$. To solve the EW equations we use the finite element method for both time (t) and space (x), whereas $\tilde{h}(x, t)$ is originally continuous. We use the first-order (Euler) discretization method which shows clean enough scaling properties to yield the critical exponents required for the EW universality class and also for the case under study here. The discretization scheme is very crucial in both growth as well as driving interface models. For the QEW model, due to its linear nature the Euler discretization scheme is enough (especially in one dimen-

sion), while for nonlinear growth models like the KPZ model, the Euler method is questionable. Due to this fact, one can see that most of the investigations on the EW and QEW models suffice to work with the Euler discretization scheme. The examples are [76–79]. We consider the effect of correlation in the quenched noise (realized by RCP) on a $L_x \times L_y$ lattice in which the interface grows on this environment. The RCP noise is defined on the lattice, and to obtain it at a point on the interface at $x = i$ (i being an integer), we calculate the integer part of h at this point to detect the integer vertical coordinate, i.e., $j = \text{int}[\tilde{h}(i, t)]$ so that the interface falls into the site (i, j) experiencing the random resisting force $\tilde{\eta}(i, j)$ to be inserted into Eq. (13).

RCP samples as the basic noise (as described in the previous section) are generated using Eq. (9) with open boundary conditions. This has been already done in our previous works with exponents consistent with the RCP universality class [40,41]. In this method, one distributes charged (white noise) impurities with normal distribution over the lattice, and the Poisson equation is solved to obtain the potential field, which serves as the quenched noise in the growth process of the interfaces. We generated more than 10^5 RCP samples and simulated the motion of one interface for each sample using Eq. (13), i.e., we have generated 10^5 interfaces for ensemble averaging. From now on, let us call the vertical direction (the y axis along which the interface grows) as the time direction and the x axis as the space direction. Generally, we need samples with more extension along the time direction since the interface needs more space to reach the steady state. In this work we considered samples with $L_y = 2 \times 10^4$, with $L_x \equiv L = 32, 64, 128, 256, 512$, and 700, space step $\Delta x = 1$ and time step $\Delta t = 0.01$, and the number of interface realizations is 10^3. The CPU time (12 cores with frequency 3.2 GHz) was $\approx 1.04 \times 10^7$ s, i.e., about 4 months.

By considering quenched noise, the interface undergoes a pinning-depinning transition that takes place at a certain critical value F_c of the driven force [see Eq. (13)].

We analyze the time dependence of the ensemble average (denoted by $\langle \cdot \rangle$ for any observable) of the mean height of the interface, i.e., $\langle \bar{h} \rangle$ in terms of the driving force F as is shown in Fig. 1(a). Although for small times $\langle \bar{h} \rangle$ varies linearly with time for all $\tilde{F}$ values, for low enough $\tilde{F}$'s at a long time limit the graphs deviate from linearity in the log-log plot, i.e., bend downwards, showing a tendency of becoming constant in long enough times, i.e., $\bar{\tilde{v}}_\infty|_{\text{low}\tilde{F}} = 0$ which is the characteristic of the pinned phase. For large $\tilde{F}$ values, however, $\langle \bar{h} \rangle$ varies linearly with time in this limit, showing that the system is in the moving phase, and a depinning phase transition takes place in between. As seen in the inset of Fig. 1(a), $\bar{\tilde{v}}_{\tilde{F}}(t, L)$ is constant for early times for all $\tilde{F}$'s, and crosses over to a new regime in the longer times which is power-law decay for low $\tilde{F}$'s and nearly constant for large $\tilde{F}$'s. For low $\tilde{F}$'s, $\bar{\tilde{v}}_{\tilde{F}}(t, L)$ falls even faster for larger times, signaling that we are in the pinned phase according to the argument given in Eq. (4) where an extra exponential decay factor is required [as mentioned in the line after Eq. (4)]. The graphs become almost constant at long times for $\tilde{F} > \tilde{F}_c$, showing that the system is in the moving phase. We have two possibilities to calculate $\bar{\tilde{v}}_\infty$ which is required for detecting the critical force $\tilde{F}_c$, which are as follows: (1) consider the velocity at the largest
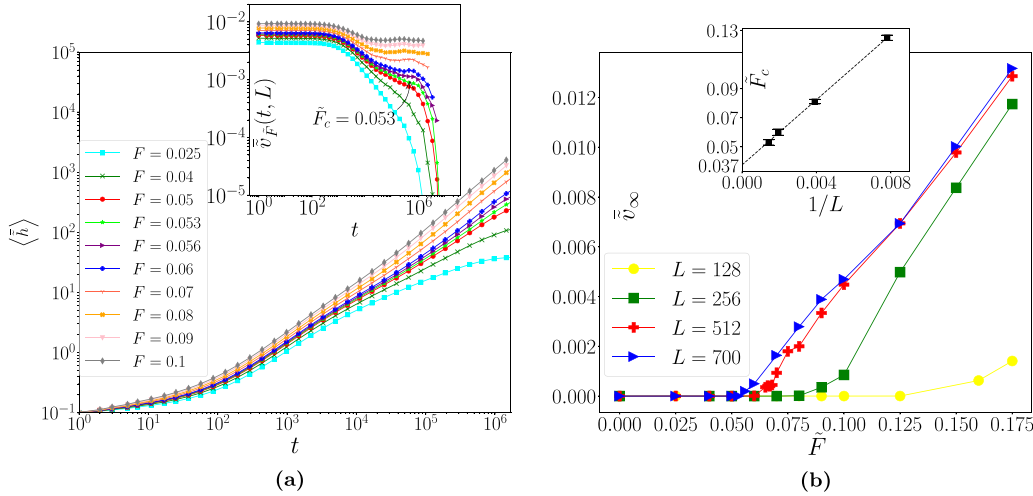
FIG. 1. (a) Log-log plots of the average height $\langle \tilde{\bar{h}} \rangle$ versus time t for various rates of the driving force $\tilde{F} = 0.025, 0.04, 0.05, 0.053, 0.056,$ $0.06, 0.07, 0.08, 0.09,$ and 0.1. In fact, the velocity strongly depends on the driving force $\tilde{F}$. The inset is log-log plots of velocity $\tilde{v}$ as a function of time t as obtained for different driving forces $\tilde{F}$ that show $\tilde{F}_c = 0.053$ that measured for a system size $L = 700$. After a short time, for $\tilde{F} > \tilde{F}_c$ the interfaces grow at a constant velocity and for $\tilde{F} < \tilde{F}_c$ the interfaces become pinned. For all figures, the results are obtained by starting with flat interfaces and averaged for 1000 realizations. (b) The plot of the velocity of growing interface for long enough times $\tilde{\bar{v}}_\infty$ versus driving force $\tilde{F}$, as measured for different system sizes L. We observe that all the interfaces become pinned below the critical point ($\tilde{\bar{v}}_\infty = 0$). The pinning-depinning transition of the interfaces takes place at critical values of driving forces of different system sizes. The inset shows critical values of driving forces $\tilde{F}_c$ vs different system sizes $\frac{1}{L}$.

time available in our data as an approximation of $\tilde{\bar{v}}_\infty$, and (2) extrapolate $\tilde{\bar{v}}_{\tilde{F}}(t, L)$ to find it. Since the extrapolation needs the precise fitting formula, the identification of which itself causes a large error (note that such a fitting formula is not clear for intermediate $\tilde{F}$'s), we considered the first strategy, and $\tilde{F}_c$ is estimated as the point where $\tilde{\bar{v}}_\infty$ becomes considerable (increases abruptly an order of magnitude) for the first time [see Fig. 1(b)]. Our statistical analysis reveals that the critical force is $\tilde{F}_c = 0.053 \pm 0.002$ for $L = 700$, which is identified by an arrow in the inset of Fig. 1(a) as the separator of the two phases. The velocity-time curve for $\tilde{F} = 0.053$ does not, however, follow a power-law behavior as is evident in this figure, and instead, the log-log plot of the orange curve ($\tilde{F} = 0.04$) is linear for two decades. To understand this we considered the finite size dependence of $\tilde{F}_c$ which is presented in Fig. 1(b), inside which $\tilde{F}_c$ is plotted as a function of $1/L$ with a nice linear fit. This analysis shows that $\tilde{F}_c$ is extrapolated linearly to 0.037 ± 0.002 as $L \to \infty$. Also we notice that $\tilde{\bar{v}}_\infty$ grows almost linearly with $\tilde{F}$ for $\tilde{F} > \tilde{F}_c$, i.e., $\theta \approx 1$ in Eq. (5).

As discussed in the arguments that led to Eq. (3), we expect that the data collapse of the roughness of the interface gives us some new exponents, i.e., α_w and z_w. In Figs. 2(a)–2(c) we show the log-log plot of $\langle \tilde{w} \rangle$ (that $\tilde{w} = \eta_{\max}^{-1} w$) versus time for different system sizes. The data collapse analysis is presented for $\tilde{F} = 0.025, 0.04,$ and 0.08 (the upper insets), each of which shows the finite size scaling hypothesis according to Eq. (3). The lower insets show the saturated roughness $\tilde{w}_{\text{sat}}$ in terms of L. The resulting exponents in terms of $\tilde{F}$ are shown in Fig. 2(d). In contrast to β_w which is nearly constant for all $\tilde{F}$ values, the exponents α_w and z_w show a change at $\tilde{F} \simeq 0.037$. For $\tilde{F} \geqslant \tilde{F}_c \simeq 0.037$, $\alpha_w \simeq 1.05 \pm 0.05$ and $z_w \simeq 1.55 \pm 0.05$, whereas for $\tilde{F} = 0.025$ (below the transition point) we have $\alpha_w = 0.852 \pm 0.05$ and $z_w = 1.32 \pm 0.05$, which are different from the corresponding exponents $\tilde{F} > \tilde{F}_c$.

For both of the phases, the obtained exponents are different from those of the EW and KPZ classes. Therefore we see that the random Coulomb potential correlated host changes the universality class of the driven interface.

Actually $\tilde{\bar{v}}_{\tilde{F}}(t, L)$ deviates from Eq. (4). To show this, let us consider the L dependence of the velocity curves in each phase, i.e., Fig. 3 where the results for $\tilde{F} = 0.025$, $\tilde{F} = 0.04$, and $\tilde{F} = 0.08$ [Figs. 3(a), 3(b), and 3(c), respectively] are shown. Interestingly we see that in all cases, the graphs cross each other in an almost *single point*, denoted by t^* which we interpret as the crossover point from pinned to moving phase. The slopes of the graphs at t^* are definitely L dependent. We see from Fig. 3(d) that $t^* \sim \tilde{F}^{-\eta}$, where $\eta = 0.64 \pm 0.04$. Also we observe that [Fig. 3(d)] $\tilde{v}^* \equiv \tilde{\bar{v}}_{\tilde{F}}(t^*, L)$ shows power-law dependence on t^* and $\tilde{F}$ consistently, i.e.,

$$\tilde{v}^* \sim t^{*-1.77 \pm 0.1} \quad \text{and} \quad \tilde{v}^* \sim \tilde{F}^{1.14 \pm 0.05}, \quad (15)$$

which is consistent with the amount of η that we found.

Before exploring the properties of t^* in more detail, let us apply the data collapse analysis based on single scaling only to the first part of the graphs ($t \ll t^*$), i.e., the relation

$$\tilde{\bar{v}}_{\tilde{F}(t \ll t^*)}(t, L) = L^{\alpha_v^{(1)}} F_{v_1}\left(\frac{t}{L^{z_v^{(1)}}}\right), \quad (16)$$

where F_{v_1} is a function with $\lim_{x \to 0} F_{v_1}(x) = \text{const.}$ v_1 represents that the analysis applies for the velocities only in the early times. This analysis, which fits only the early parts of the graphs, is shown in the lower insets, the results of which are shown in Table I. We see that the exponents do not vary with $\tilde{F}$.

It is important to note, however, that all parts of the velocity are not fitted with this relation, i.e., the portions in longer times are different. The most optimal way out of this inconsistency is to consider a scaling relation with *two vari-*
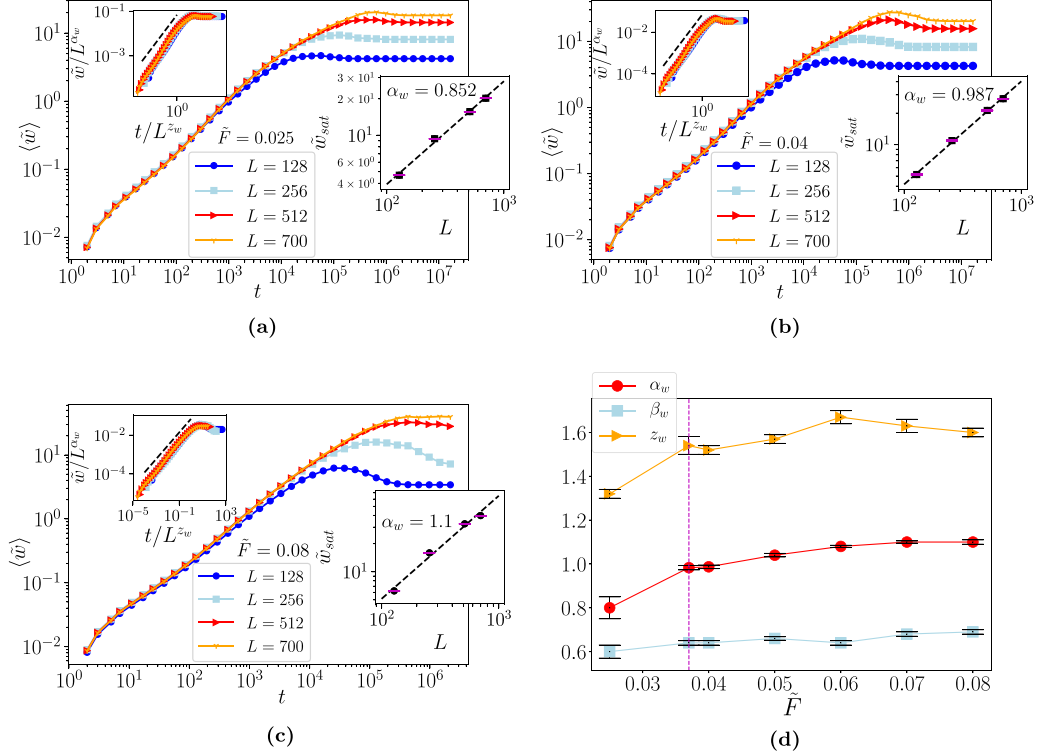
FIG. 2. Log-log plots of the average interface width $\langle \tilde{w} \rangle$ versus time t for different sizes L. From the best fit of the data in the inset, we obtain the following: (a) For $\tilde{F} = 0.025$, $\alpha_w = 0.852 \pm 0.05$, $z_w = 1.32 \pm 0.02$ and $\beta_w = 0.6 \pm 0.03$. (b) For $\tilde{F} = 0.04$, $\alpha_w = 0.987 \pm 0.008$, $z_w = 1.52 \pm 0.02$, and $\beta_w = 0.64 \pm 0.01$. (c) For $\tilde{F} = 0.08$, $\alpha_w = 1.10 \pm 0.01$, $z_w = 1.6 \pm 0.02$, and $\beta_w = 0.69 \pm 0.01$. Right-hand side insets: Log-log plot of interface width during the saturation regime ($\tilde{w}_{\text{sat}}$) as a function of the system size L (data obtained from the main figure for $t \geqslant t_X$). (d) We plot α_w, β_w, and z_w exponents in terms of $\tilde{F}$ and the dashed line shows $F_c = 0.037$.

ables. To understand this, let us recall that there are two relevant spatial scales, namely, the system size L and the correlation length $\xi_{\tilde{F}}$. This correlation length is related to the correlation time which is given by the time dependence of the velocity [see one line below Eq. (4)] and accordingly a correlation length which is $\zeta = \bar{v}\xi_F$. This correlation becomes infinity (more precisely of the order of the length of the lattice for finite systems) right at the depinning transition point, so that Eq. (4) is obtained which includes no characteristic length scale. The correlation length behaves like $\xi_{\tilde{F}}^{\infty} \equiv \xi_{\tilde{F}}^{L \to \infty} \sim (\tilde{F} - \tilde{F}_c)^{-\nu}$ in the thermodynamic limit close to the continuous transition points. This, alongside the fact that $\bar{\bar{v}}_{\tilde{F}}(t, L)$ is L independent at t^* implies that the velocity is in the form

$$\bar{\bar{v}}_{\tilde{F}}(t, L) = L^{-\alpha_v} G\left(\frac{t - t^*}{L^{z_1}}, \frac{t}{L^{\beta_v} \xi_{\tilde{F}}^{\infty z_2}} \right), \quad (17)$$

TABLE I. Numerical results for exponents of interface velocity in different phases in near critical point.

Quantity	α_v	z_v	$\beta_v = \frac{\alpha_v}{z_v}$
$\tilde{F} = 0.025$	0.15 ± 0.04	0.42 ± 0.05	0.34 ± 0.06
$\tilde{F} = 0.04$	0.14 ± 0.04	0.42 ± 0.05	0.32 ± 0.06
$\tilde{F} = 0.08$	0.13 ± 0.03	0.42 ± 0.05	0.31 ± 0.04

where α_v, β_v, z_1, and z_2 are scaling exponents. We propose (and confirm later) that $G(x, y)$ asymptotically behaves like

$$G(0, y) \sim y^{-\alpha_v / \beta_v}, \quad G(-x, 0) \sim a'x^{-\gamma} + b, \quad (18)$$

where γ is a new exponent, and a' and b are some nonuniversal constants. Therefore, at $t = t^*$ we have

$$\bar{\bar{v}}_{\tilde{F}}(t^*, L) \propto \left(\xi_{\tilde{F}}^{\infty} \right)^{\alpha_v z_2 / \beta_v} t^{*-\alpha_v / \beta_v} \quad \text{(independent of } L\text{)} \quad (19)$$

and also

$$\lim_{t \to 0} \bar{\bar{v}}_{\tilde{F}}(t, L) = a'L^{-\alpha_v + \gamma z_1} t^{*-\gamma} + bL^{-\alpha_v}. \quad (20)$$

To fix these exponents, we analyzed $\bar{\bar{v}}_{\tilde{F}}(0, L)$ in terms of L for fixed $\tilde{F}$ (and consequently fixed t^*), the results of which are shown in Fig 4. Figure 4(a) shows the dependence on $\tilde{F}$, which reveals that $\bar{\bar{v}}_{\tilde{F}}(0, L)$ is linear with respect to $\tilde{F}$. Therefore, recalling that $t^* \propto \tilde{F}^{-\eta}$, one obtains $\gamma = \frac{1}{\eta} = 1.56 \pm 0.09$. This illustrates that

$$\lim_{t \to 0} \bar{\bar{v}}_{\tilde{F}}(t, L) = m_L^{(1)} \tilde{F} + m_L^{(2)}, \quad (21)$$

where $m_L^{(1)} = aL^{-\alpha_v + (z_1/\eta)}$ and $m_L^{(2)} = bL^{-\alpha_v}$, and a is a nonuniversal constant. The dependence of these slopes on L is shown in Fig. 4(b), giving $\alpha_v = 0.39 \pm 0.09$ and $z_1 = 0.29 \pm 0.07$.

The only remaining exponents are z_2 and β_v, which are obtained by analyzing $\tilde{v}^*$. Since $\tilde{v}^* \equiv \bar{\bar{v}}_{\tilde{F}}(t^*, L)$ does not vanish, or become divergent at $\tilde{F}_c$ that we have found above (does not
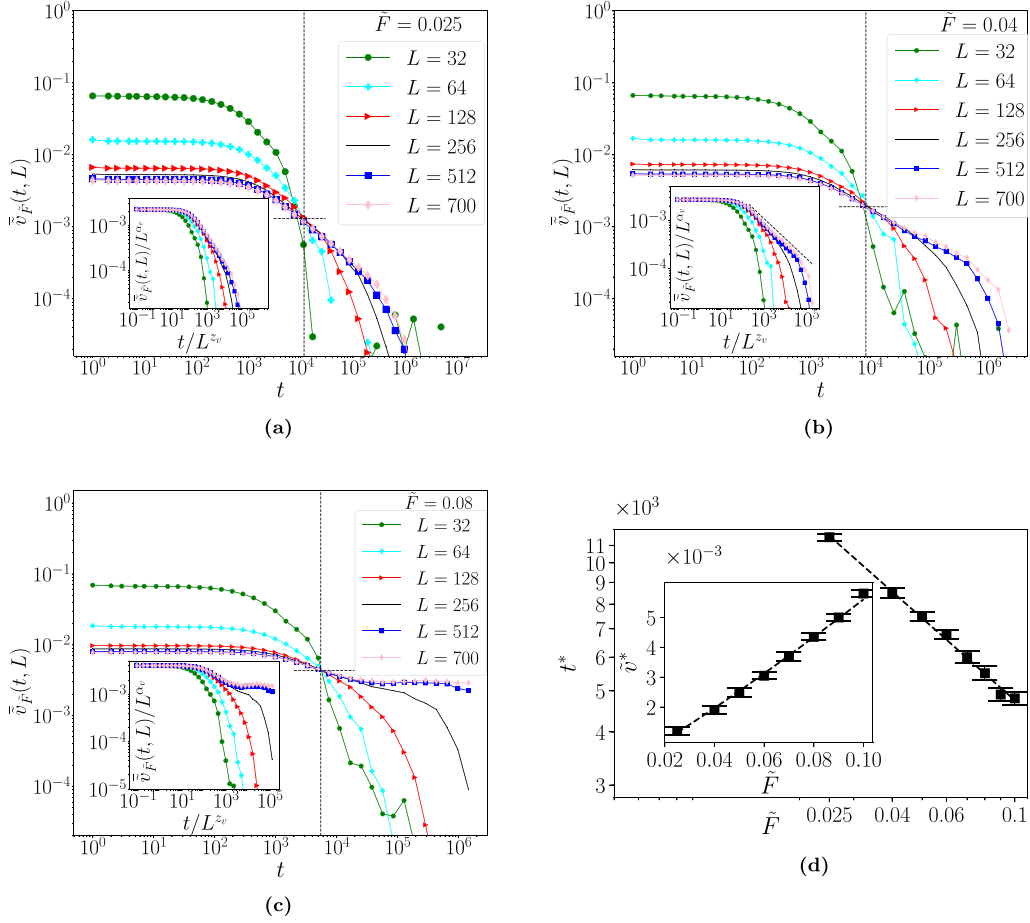
FIG. 3. (a) Log-log plots of $\bar{\tilde{v}}_{\tilde{F}}(t, L)$ versus t at the driving force $\tilde{F} = 0.025$, as measured for different system sizes L (all sizes are in pinned phase). (b) Log-log plots of $\bar{\tilde{v}}_{\tilde{F}}(t, L)$ versus t for $\tilde{F} = 0.04$. (c) Log-log plots of $\bar{\tilde{v}}_{\tilde{F}}(t, L)$ versus t for $\tilde{F} = 0.08$. Numerical results for exponents of interface velocity in different phases are given in Table I. (d) Log-log plot t^* time in the crossover point versus $\tilde{F}$ and the inset is log-log plot $\tilde{v}^*$ versus $\tilde{F}$ for a system size $L = 700$.

depend on $\xi_{\tilde{F}}^{\infty}$), we conclude that $z_2 = 0$, giving rise to

$$\tilde{v}^* \sim t^{*-\alpha_v/\beta_v}. \tag{22}$$

Using Eq. (15) we find that $\beta_v = 0.22 \pm 0.07$. These exponents are shown in Table II.

As an important check for the validity of Eq. (17), we study the slope of $\bar{\tilde{v}}_{\tilde{F}}(t, L)$ in the vicinity of t^*. Consider two variables $x \equiv L^{-z_1}(t - t^*)$ and $y \equiv t \xi_{\tilde{F}}^{-z_2} L^{-\beta_v}$ so that $(x^*, y^*) \equiv (0, \frac{t^*}{L^{\beta_v} \xi_{\tilde{F}}^{z_2}})$ is the crossover point, so that (noting from the above that t^* is only $\tilde{F}$ dependent) $\tilde{v}_{\tilde{F}}(x^*, y^*)$ is apparently
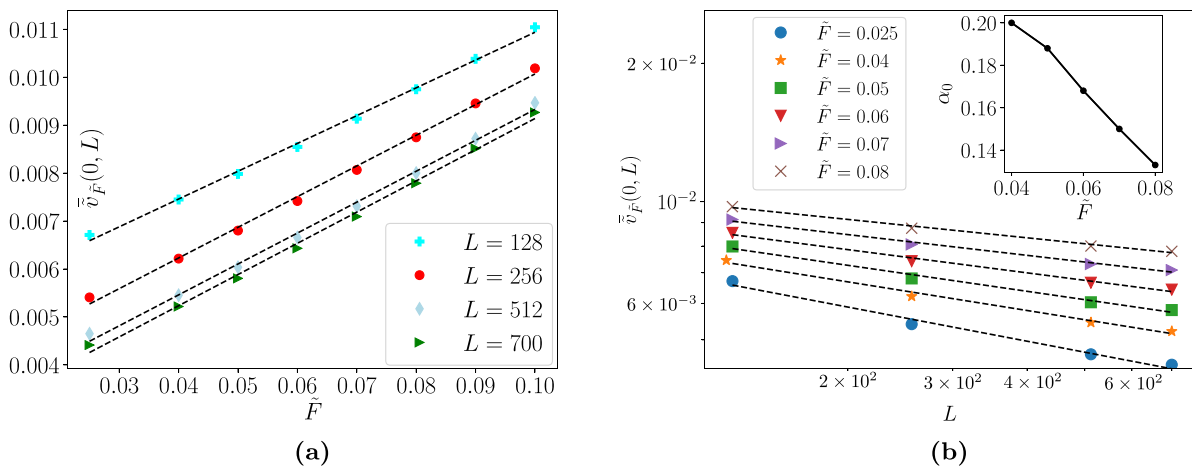

FIG. 4. (a) The log-log plot of $\bar{\tilde{v}}_{\tilde{F}}(0, L)$ in terms of (a) $\tilde{F}$ and (b) L with the exponents shown in the inset.
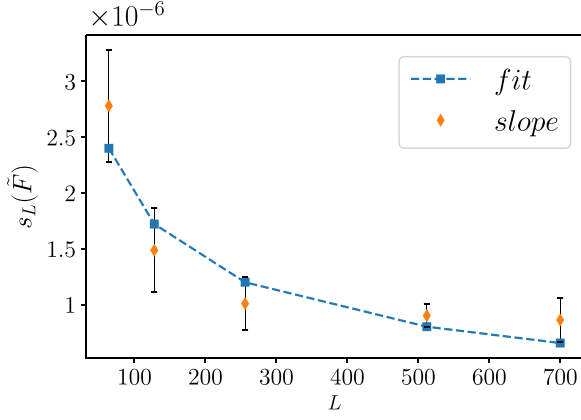
FIG. 5. The dependence of $s_L(\tilde{F})$ versus L for $\tilde{F} = 0.04$. The dashed line is the fitting with the exponents $z_1 = 0.3 \pm 0.04$, $\beta_v = 0.2 \pm 0.03$, and $z_2 = 0$ according to Eq. (25).

L independent. One can expand $\bar{\bar{v}}_{\tilde{F}}(t, L)$ in the vicinity of x^* and y^*, giving rise to

$$\bar{\bar{v}}_{\tilde{F}}(t, L) = \tilde{v}^* + (t - t^*)\left(\frac{A_{\tilde{F}}(L)}{L^{z_1}} + \frac{B_{\tilde{F}}(L)}{L^{\beta_v}\xi_{\tilde{F}}^{z_2}}\right) + \cdots, \quad (23)$$

where $A_L(\tilde{F}) \equiv \partial_x G(x^*, y^*) = A(\frac{t^*}{L^{\beta_v}\xi_{\tilde{F}}^{z_2}})$ and $B_L(\tilde{F}) \equiv \partial_y G(x^*, y^*) = B(\frac{t^*}{L^{\beta_v}\xi_{\tilde{F}}^{z_2}})$ are the expansion coefficients. We then have

$$\bar{\bar{v}}_{\tilde{F}}(t, L) - \tilde{v}^* \propto s_L(\tilde{F})(t - t^*), \quad (24)$$

where

$$s_L(\tilde{F}) = \frac{A_L(\tilde{F})}{L^{z_1}} + \frac{B_L(\tilde{F})}{L^{\beta_v}\xi_{\tilde{F}}^{z_2}}. \quad (25)$$

The fact that $A_L(\tilde{F})$ and $B_L(\tilde{F})$ are L and $\tilde{F}$ dependent, makes this analysis hard to do. For $\tilde{F} \simeq \tilde{F}_c$, however, we found that these dependencies are negligible, and the obtained exponents are very close to the ones found above. The result is shown in Fig. 5, in which the exponents are shown, i.e., $\beta_v = 0.2 \pm 0.03$ and $z_1 = 0.3 \pm 0.04$, which are consistent with the fittings just found in our previous analysis. From

TABLE II. The exponents of the velocity, given in Eq. (17).

α_v	β_v	γ	z_1	z_2	η
0.39(9)	0.22(7)	1.56(9)	0.29(7)	0	0.64(4)

this study we infer that there is a crossover from $L < L^*$ to $L > L^*$, where $L^* = (A/B)^{1/(z_1-\beta)}\xi_{\tilde{F}}^{z_2/(z_1-\beta)}$. More precisely for $L > L^*$ we expect that the slope is given by $BL^{-\beta}\xi_{\tilde{F}}^{-z_2}$, whereas for $L < L^*$ it is AL^{-z_1}.

Now let us consider the velocities in the tilted setup, i.e., Eq. (7), using which one can determine the universality classes. Figure 6 presents the results (the average velocity $\bar{\bar{v}}_\infty$) of the setup in which the initial interface is tilted with a slope m for various driving forces, and for a system size $L = 700$. This figure shows that v varies almost linearly with m^2 [Fig. 6(a)], especially in large m^2 values which confirms the relation (7). We use the data collapse technique using the relation (8), which is shown in the inset of Fig. 6(a). With a simple rescaling $\frac{\bar{\bar{v}}_\infty}{f}$ and $\frac{m^2}{f^{1/4}}$. We see that the curves fit to each other. It is seen that θ is almost 1, and $1 - \phi = 0.25$, giving rise to $\phi \approx \frac{3}{4}$. This shows that the λ term does not diverge in the thermodynamic limit as the KPZ universality class. The F dependence of λ is depicted in Fig. 6(b) in the vicinity of $\tilde{F}_c \approx 0.081$ for $L = 256$, from which we see a nearly constant λ. For the $\tilde{F}_c$ this slope is a monotonic decreasing function of L, and extrapolates to zero in the $L \to \infty$ limit. This analysis shows again that the nonlinearity term (which is responsible for lateral growth in KPZ) is not present in our model.

V. CONCLUDING REMARKS

In this paper, we considered the effect of correlation in the (quenched) noise on a $L_x \times L_y$ square lattice to the depinning transition and observed that it has a nontrivial effect on the motion and the morphology of an interface. To this end, we considered the dynamics of interfaces which are described by the QEW driven by the force $\tilde{F}$ on top of a lattice in which the noise results from a random Coulomb
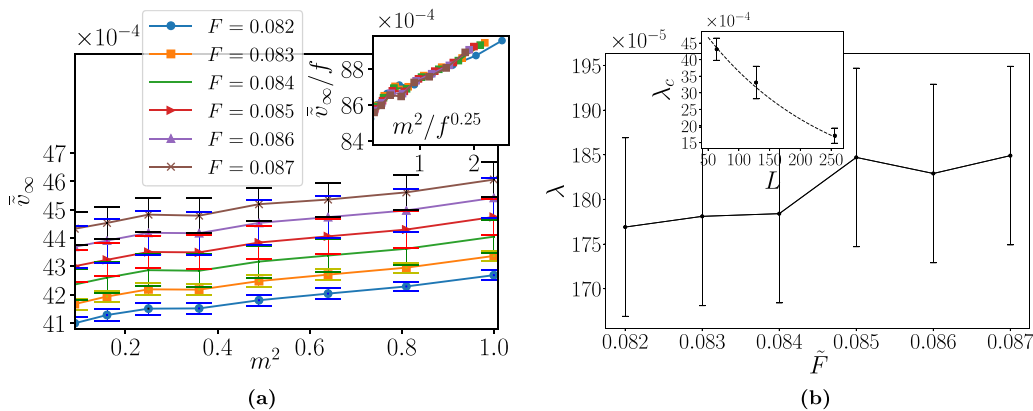

FIG. 6. (a) The dependence of $\bar{\bar{v}}_\infty$ of the tilted setup in terms of m^2. Inset: data collapse analysis of the main panel. (b) The slope of the $\bar{\bar{v}}_\infty - m^2$ relation in terms of $\tilde{F}$, i.e., $\lambda(\tilde{F})$. Inset shows $\lambda_c \equiv \lambda(\tilde{F}_c)$ in terms of the system size L, which decreases with L, extrapolating to zero as $L \to \infty$.

potential noise (which corresponds to the two-dimensional Edwards-Wilkinson model in the stationary regime). The interface is shown to be pinned by disorder if the driving force is small, and there is a critical force, shown by $\tilde{F}_c$ where the interfaces are critically pinned, so that for the forces just above this critical force the interface advances by jumping from one pinning path to another with a velocity almost proportional to $\tilde{F}$ [see Fig. 1(b) that shows the final velocity $\bar{\tilde{v}}_\infty$]. In the vicinity of the transition point the velocity varies according to Eq. (5) with $\theta \approx 1$. In the moving phase, i.e., very large driving forces ($\tilde{F} \gg \tilde{F}_c$),

the velocity of the interfaces is proportional to the driving force (the interfaces grow with constant speed). The analysis of the roughness shows that the growth exponents of our model are $\alpha_w = 1.05 \pm 0.01$ and the dynamical exponent $z_w = 1.55 \pm 0.05$, showing that the system is in a new universality class which is different from both EW and KPZ.

We also developed a two-variable scaling analysis for the velocity which is based on the observation of a crossover point where the velocity becomes L independent. The exponents of this analysis are reported in Table II.

[1] L. M. Pismen, *Patterns and Interfaces in Dissipative Dynamics* (Springer Science & Business Media, New York, 2006).

[2] P. Collet and J.-P. Eckmann, *Instabilities and Fronts in Extended Systems* (Princeton University Press, Princeton, NJ, 2014), Vol. 44.

[3] M. C. Cross and P. C. Hohenberg, Rev. Mod. Phys. **65**, 851 (1993).

[4] K. Singh, M. Jung, M. Brinkmann, and R. Seemann, Annu. Rev. Fluid Mech. **51**, 429 (2019).

[5] F. D. Reis, Braz. J. Phys. **33**, 501 (2003).

[6] Luis A. Nunes Amaral, A.-L. Barabási, H. A. Makse, and H. E. Stanley, Phys. Rev. E **52**, 4087 (1995).

[7] A. Scanziani, Q. Lin, A. Alhosani, M. J. Blunt, and B. Bijeljic, Proc. R. Soc. A **476**, 20200040 (2020).

[8] Q. Zhu, Q. Zhou, and X. Li, J. Rock Mech. Geotech. Eng. **8**, 87 (2016).

[9] M. Hashemi, B. Dabir, and M. Sahimi, AIChE J. **45**, 1365 (1999).

[10] H. S. Rabbani, V. Joekar-Niasar, T. Pak, and N. Shokri, Sci. Rep. **7**, 4584 (2017).

[11] A. Szymkiewicz, *Modelling Water Flow in Unsaturated Porous Media* (Springer, New York, 2013), pp. 9–47.

[12] R. T. Armstrong, N. Evseev, D. Koroteev, and S. Berg, Adv. Water Resour. **77**, 57 (2015).

[13] G. Pahar and A. Dhar, Eng. Anal. Boundary Elem. **68**, 75 (2016).

[14] S. Atis, A. K. Dubey, D. Salin, L. Talon, P. Le Doussal, and K. J. Wiese, Phys. Rev. Lett. **114**, 234502 (2015).

[15] A. S. Balankin, H. Zapata López, E. Pineda León, D. Morales Matamoros, L. Morales Ruiz, D. Silva López, and M. A. Rodríguez, Phys. Rev. E **87**, 014102 (2013).

[16] J. Yang and E. S. Boek, Comput. Math. Appl. **65**, 882 (2013).

[17] M. A. Rubio, C. A. Edwards, A. Dougherty, and J. P. Gollub, Phys. Rev. Lett. **63**, 1685 (1989).

[18] V. K. Horváth, F. Family, and T. Vicsek, Phys. Rev. Lett. **67**, 3207 (1991).

[19] B. K. Primkulov, A. A. Pahlavan, X. Fu, B. Zhao, C. W. MacMinn, and R. Juanes, J. Fluid Mech. **875** (2019).

[20] J. Zhang, Y. C. Zhang, P. Alstrøm, and M. T. Levinsen, Physica A **189**, 383 (1992).

[21] G. Blatter, M. V. Feigel'man, V. B. Geshkenbein, A. I. Larkin, and V. M. Vinokur, Rev. Mod. Phys. **66**, 1125 (1994).

[22] R. Allenspach, M. Stampanoni, and A. Bischof, Phys. Rev. Lett. **65**, 3344 (1990).

[23] B. Moglia, E. V. Albano, and N. Guisoni, Phys. Rev. E **94**, 052139 (2016).

[24] J. H. Lee, S. K. Kim, and J. M. Kim, Phys. Rev. E **62**, 3299 (2000).

[25] A.-L. Barabási and H. E. Stanley, *Fractal Concepts in Surface Growth* (Cambridge University Press, Cambridge, UK, 1995).

[26] A. Brú, S. Albertos, J. A. López García-Asenjo, and I. Brú, Phys. Rev. Lett. **92**, 238101 (2004).

[27] J. A. Bonachela, C. D. Nadell, J. B. Xavier, and S. A. Levin, J. Stat. Phys. **144**, 303 (2011).

[28] Y. Azimzade, A. A. Saberi, and M. Sahimi, Phys. Rev. E **100**, 062409 (2019).

[29] L.-H. Tang and H. Leschhorn, Phys. Rev. A **45**, R8309 (1992).

[30] H. Leschhorn, Phys. Rev. E **54**, 1313 (1996).

[31] N. Şenbil, M. Gruber, C. Zhang, M. Fuchs, and F. Scheffold, Phys. Rev. Lett. **122**, 108002 (2019).

[32] A. B. Kolton and E. A. Jagla, Phys. Rev. E **98**, 042111 (2018).

[33] P. M. Adler and J.-F. Thovert, *Fractures and Fracture Networks* (Springer Science & Business Media, New York, 1999), Vol. 15.

[34] H. Hardy and R. A. Beier, *Fractals in Reservoir Engineering* (World Scientific, Singapore, 1994).

[35] W. Wang, A. G. Cherstvy, X. Liu, and R. Metzler, Phys. Rev. E **102**, 012146 (2020).

[36] J. Zierenberg, N. Fricke, M. Marenz, F. P. Spitzner, V. Blavatska, and W. Janke, Phys. Rev. E **96**, 062125 (2017).

[37] M. Sahimi, Rev. Mod. Phys. **65**, 1393 (1993).

[38] S. Hosseinabadi, M. A. Rajabpour, M. S. Movahed, and S. M. Vaez Allaei, arXiv:1304.2219.

[39] D. Bernard, G. Boffetta, A. Celani, and G. Falkovich, Phys. Rev. Lett. **98**, 024501 (2007).

[40] J. Cheraghalizadeh, M. N. Najafi, and H. Mohammadzadeh, Eur. Phys. J. B **91**, 81 (2018).

[41] J. Cheraghalizadeh, M. Najafi, and H. Mohammadzadeh, J. Stat. Mech. (2018) 083301.

[42] P. Francesco, P. Mathieu, and D. Sénéchal, *Conformal Field Theory* (Springer Science & Business Media, New York, 2012).

[43] J. Cardy, Ann. Phys. **318**, 81 (2005).

[44] H. Stanley, S. Buldyrev, A. Goldberger, S. Havlin, C.-K. Peng, and M. Simons, Physica A **200**, 4 (1993).

[45] M. A. Knackstedt, M. Sahimi, and A. P. Sheppard, Phys. Rev. E **61**, 4920 (2000).

[46] E. Daryaei, Phys. Rev. E **101**, 062108 (2020).

[47] T. Song and H. Xia, Phys. Rev. E **103**, 012121 (2021).

[48] K. Fujimoto, R. Hamazaki, and Y. Kawaguchi, Phys. Rev. Lett. **124**, 210604 (2020).

[49] U. C. Täuber and M. Pleimling, Phys. Rev. E **101**, 022101 (2020).

[50] K. A. Takeuchi, Physica A **504**, 77 (2018).

[51] M. G. Nezhadhaghighi and M. A. Rajabpour, Phys. Rev. E **83**, 021122 (2011).

[52] M. N. Najafi and M. G. Nezhadhaghighi, Phys. Rev. E **95**, 032112 (2017).

[53] L. A. Braunstein and C.-H. Lam, Phys. Rev. E **72**, 026128 (2005).

[54] A. Kolakowska, M. A. Novotny, and P. S. Verma, Phys. Rev. E **73**, 011603 (2006).

[55] Y.-L. Chou and M. Pleimling, Phys. Rev. E **79**, 051605 (2009).

[56] J. P. Stokes, A. P. Kushnick, and M. O. Robbins, Phys. Rev. Lett. **60**, 1386 (1988).

[57] V. K. Horváth, F. Family, and T. Vicsek, J. Phys. A: Math. Gen. **24**, L25 (1991).

[58] S. V. Buldyrev, A.-L. Barabási, F. Caserta, S. Havlin, H. E. Stanley, and T. Vicsek, Phys. Rev. A **45**, R8313 (1992).

[59] L. A. N. Amaral, A.-L. Barabási, S. V. Buldyrev, S. Havlin, and H. E. Stanley, Phys. Rev. Lett. **72**, 641 (1994).

[60] L. A. N. Amaral, A.-L. Barabási, S. V. Buldyrev, S. T. Harrington, S. Havlin, R. Sadr-Lahijany, and H. E. Stanley, Phys. Rev. E **51**, 4655 (1995).

[61] J. Krug, Phys. Rev. A **44**, R801 (1991).

[62] P. Grassberger, Phys. Rev. Lett. **120**, 200605 (2018).

[63] Luis A. Nunes Amaral, A.-L. Barabási, and H. E. Stanley, Phys. Rev. Lett. **73**, 62 (1994).

[64] B. Moglia, E. V. Albano, P. Villegas, and M. A. Muñoz, J. Stat. Mech. (2014) P10024.

[65] M. Sahimi and S. E. Tajer, Phys. Rev. E **71**, 046301 (2005).

[66] Y. Gefen, B. B. Mandelbrot, and A. Aharony, Phys. Rev. Lett. **45**, 855 (1980).

[67] J. Cheraghalizadeh, M. N. Najafi, H. Dashti-Naserabadi, and H. Mohammadzadeh, Phys. Rev. E **96**, 052127 (2017).

[68] M. Najafi, J. Phys. A: Math. Theor. **49**, 335003 (2016).

[69] M. Najafi, Phys. Lett. A **380**, 370 (2016).

[70] M. Najafi, M. Ghaedi, and S. Moghimi-Araghi, Physica A **445**, 102 (2016).

[71] M. N. Najafi, J. Physica A: Mathe. Theore. **51**, 175001 (2018).

[72] J. Kondev and C. L. Henley, Phys. Rev. Lett. **74**, 4580 (1995).

[73] P. Francesco, P. Mathieu, and D. Sénéchal, *Conformal Field Theory* (Springer, New York, 1996).

[74] R. J. Adler, *The Geometry of Random Fields* (Society for Industrial and Applied Mathematics, Philadelphia, 1981), Vol. 62.

[75] M. Najafi and M. Ghaedi, Physica A **427**, 82 (2015).

[76] J. M. Kim and H. Choi, J. Korean Phys. Soc. **48**, 241 (2006).

[77] K. Park and I.-m. Kim, Phys. Rev. E **59**, 5150 (1999).

[78] E. E. Ferrero, S. Bustingorry, and A. B. Kolton, Phys. Rev. E **87**, 032122 (2013).

[79] N. Caballero, E. Agoritsas, V. Lecomte, and T. Giamarchi, Phys. Rev. B **102**, 104204 (2020).